XPS Investigation of the Electrolyte Induced Stabilization of LiCoO[subscript 2] and "AlPO[subscript 4]"-Coated LiCoO[subscript 2] Composite electrodes

XPS Investigation of the Electrolyte Induced Stabilization of $LiCoO_2$ and "$AlPO_4$"-Coated $LiCoO_2$ Composite Electrodes

Ronald A. Quinlan,[a,c] Yi-Chun Lu,[b,*,d] David Kwabi,[b] Yang Shao-Horn,[b,*] and Azzam N. Mansour[a,*,z]

[a]*The Naval Surface Warfare Center, Carderock Division, West Bethesda, Maryland 20817, USA*
[b]*Electrochemical Energy Laboratory, Massachusetts Institute of Technology, Cambridge, Massachusetts 02139, USA*

The "$AlPO_4$" coating has been shown to improve the electrochemical performance of $LiCoO_2$ batteries. We previously showed that the "$AlPO_4$" coating promotes the formation of metal fluorides, which could act as a stable surface film and protect $LiCoO_2$ from continuous degradation upon cycling. In this work, we removed the fluorine source in the $LiPF_6$ salt by using the $LiClO_4$ salt and investigated the effectiveness of the "$AlPO_4$" coating. Interestingly, the "$AlPO_4$" coating was found to improve the voltage efficiency and capacity retention when cycling in the $LiPF_6$ electrolyte, but was detrimental when cycling in the $LiClO_4$ electrolyte. XPS revealed that the "$AlPO_4$" coating promotes the formation of metal fluoride in both electrolytes, with the surface film formed in $LiClO_4$ being more electrically resistive compared to that formed in $LiPF_6$. The source of fluorine in the coated electrode cycled in $LiPF_6$ is largely attributed to the $LiPF_6$ salt whereas the source of fluorine in the coated electrode cycled in $LiClO_4$ is the binder PVDF. We believe that the coating could react with HF impurity in the $LiPF_6$ electrolyte or from the binder PVDF and form stable metal fluoride films on the surface.
 [DOI: 10.1149/2.0851602jes] All rights reserved.

Manuscript submitted August 24, 2015; revised manuscript received November 16, 2015. Published December 3, 2015.

Lithium cobalt oxide, $LiCoO_2$, is currently the most common cathode material used in lithium ion battery technology,[1,2] but only half of the theoretical capacity, ≈140 mA h g^{-1}, is obtained when charged to 4.2 V vs. Li^+/Li. Higher capacity is obtainable if cycled to voltages greater than 4.2 V, but this was shown to result in high capacity loss.[3,4] Structural instability[3,5] and reactivity of the cathode with the electrolyte[3] have both been proposed as possible mechanisms for the observed capacity fade. Surface modification via coatings with intrinsic materials by thermal treatment during the synthesis process[6] or with extrinsic materials,[7–10] is one successful method of improving performance. These cathodes with surface-modified $LiCoO_2$[1,2,6–11] have shown improvement when cycled to high voltages compared to bare $LiCoO_2$ positive electrodes. However, the origin responsible for the increased performance is not well understood. Understanding the mechanism responsible for the enhancement in cycling stability provided by the coatings/surface modification is essential to further stabilize positive electrode materials for applications that demand high cycle life such as electrical vehicles and stationary storage.

Enhanced performance in cycling associated with surface coating has been attributed to phase transitions,[3,4,12–15] coatings,[3,5,15,16] suppression of electrolyte decomposition, reduced oxygen activity associated with cation mixing,[3,17–19] physical barriers and HF scavenging,[6,19–21] suppression of side reactions,[7–10,22,23] electrolyte acidity,[16,24] and the PVDF binder as a source of HF.[25,26] The recent investigation by Dahèron et al.,[18] showed that the substitution of Al for Co not only increases the ionic nature of the Co-O bond through orbital mixing, but also that the substitution reduces the basicity of the $LiCoO_2$ surface, thus making the surface less receptive or vulnerable to acidic attack in the electrolyte. However, this benefit can be temporary as recent work indicates that the Li-Al-Co-O surface region is consumed during cycling.[27] The "$AlPO_4$"-coating on $LiCoO_2$ can induce the formation of Al-rich regions ($LiAl_yCo_{1-y}O_2$) and P-rich regions (Li^+ conducting Li_3PO_4),[28] and that Co- and Al-containing oxyfluoride species and species like $PF_x(OH)_y$ developed on the surface during cycling can lower the rate of Co dissolution and deposition of Co-containing species on the negative electrode and further degradation of $LiPF_6$.[27] For a more detailed discussion of the metal fluoride formation mechanism, the reader is directed to Figure 12 and the corresponding discussion in the report by Lu et al.[27]

In this paper, we examine the influence of the fluorine source on the formation of metal fluorides and the efficacy of the surface coating by relating cycling performance to the surface chemistries of bare and "$AlPO_4$"-coated $LiCoO_2$ electrodes cycled in 1 M $LiPF_6$ or $LiClO_4$ in EC:DMC (1:1) to 4.6 V. For a more detailed discussion of the metal fluoride formation mechanism, the reader is directed to Figure 12 and the corresponding discussion on page 4421 (second column) of Lu et al.[27] The $LiClO_4$ salt was used to help determine if the formation of the metal fluorides was a product of the interaction between the active material with the $LiPF_6$ electrolyte and/or the PVDF binder. The contribution of the F-containing $LiPF_6$ salt on the efficacy of the surface coating in contrast to the non F-containing $LiClO_4$ salt will be discussed.

Experimental

Bare $LiCoO_2$ and "$AlPO_4$"-coated $LiCoO_2$ powder samples were prepared as previously described.[28] The reversible capacities and cycling stability of bare and "$AlPO_4$"-coated $LiCoO_2$ composite electrodes were measured by using a two-electrode lithium cell (Tomcell type TJ-AC). Lithium cells were constructed inside the glove box (H_2O, O_2 < 0.1 ppm, Mbraun, USA) using a lithium metal foil as the negative electrode and the composite positive electrode separated by two polypropylene microporous separators (Celgard 2500). The electrolytes used were 1 M $LiPF_6$ or 1 M $LiClO_4$ (battery grade, dry, 99.99% trace metals basis, Aldrich) in a 3:7 volume ratio EC/DMC solvent (Kishida Chemical Corp, Japan). The assembled lithium cells were set aside for 6 h prior to electrochemical testing on a Solartron 1470 battery testing unit in order for the electrolyte to wet the electrodes. The cells with bare and coated $LiCoO_2$ electrodes were cycled at the C/5 rate between voltage limits of 2.0–4.6 V with 4 h hold at 4.6 V for 20 cycles. The C-rate was defined based on the theoretical capacity of $LiCoO_2$ (274 mA h g^{-1}). The discharged cells were disassembled in the glove box, after which the Li_xCoO_2 electrodes were extracted and stored in hermetically sealed containers in the glove box.

The XPS spectra of bare and "$AlPO_4$"-coated $LiCoO_2$ electrodes before and after cycling were measured using a Physical Electronics model 5400 X-ray photoelectron spectrometer. Each electrode was removed from the hermetically sealed container in an argon-filled glove box (< 3 ppm O_2, < 3.5 ppm H_2O) and mounted onto the sample puck

*Electrochemical Society Active Member.
[c]Present Address: Molecular Biology and Chemistry, Christopher Newport University, Newport News, Virginia 23606, USA.
[d]Present Address: Mechanical and Automation Engineering, The Chinese University of Hong Kong, Shatin, NT, Hong Kong.
[z]E-mail: azzam.mansour@navy.mil

with the aid of copper clips placed on the edge of the electrode. The electrode was then transferred via a sealed chamber to the introduction chamber of the XPS spectrometer without exposure to ambient conditions. The introduction chamber was evacuated for 10–15 min before the sealed chamber was opened, then the sealed chamber was opened and evacuated for another 10–15 min before transferring the sample to the analysis chamber. The data were collected at room temperature using non-monochromatic Al Kα (1486.6 eV) X-ray source operating at 400 W (15 kV and 27 mA). Data collection proceeded when the pressure in the analysis chamber reached $\approx 2\times10^{-8}$ Torr. Survey spectra (0 – 900 eV at an electron takeoff angle of 45°) were collected at analyzer pass energy of 89.45 eV with energy resolution of 1.34 eV, 0.5 eV/step and an integration interval of 50 ms/step. The survey spectra consist of the average of 20 cycles with total acquisition time of 30.42 min. Multiplex spectra were collected at analyzer pass energy of 35.75 eV with energy resolution of 0.54 eV, 0.2 eV/step and an integration interval of 50 ms/step. The binding energies for the pristine (bare and coated) electrodes are reported as measured since there was no indication of electrode charging as indicated by the binding energy of the C 1s line for carbon black at 284.4 eV, which is in close agreement with a number of previously reported results.[29,30] The cycled electrodes displayed a small degree of charging in the range of 0.2–0.4 eV, but their binding energies are reported with respect to carbon black at 284.4 eV. The binding energies of reference compounds in powder form are reported with respect to hydrocarbon at 285.0 eV. These procedures yielded the same binding energies for the C 1s and F 1s lines for powder PVDF and an electrode, which consisted of a mixture of PVDF and carbon black.

Depth profile analyses were made using 4 keV Ar ions with a raster size of 4×4 mm^2. The sputtering was made in 0.5 or 1 minute intervals for a total sputtering time of 6 minutes. The C 1s, O 1s, F 1s, Li 1s, Co 2p, P 2p and Cl 2p photoemission lines were collected after each interval of sputtering at analyzer pass energy of 35.75 eV and an energy increment of 0.2 eV. The sputtering rate was calibrated using a 1000 Å SiO_2 film on a Si substrate and was found to be in the range of 25–30 Å of SiO_2 per minute.

Another set of XPS spectra were collected on beamline X24A of the National Synchrotron Light Source utilizing monochromatic X-rays with energy of 2555 eV compared to 1486.6 eV for Al K_α X-rays in order to increase the depth of the analyzed region. The experimental setup consisted of a 2-stage high vacuum chamber with base pressure below 10^{-7} Torr and a Scienta R4000 detector running in transmission mode at pass energy of 200 eV with 0.3 mm analyzer aperture. The pass energy and aperture combination gives a resolution of about 0.29 eV at beam energy of 2139 eV as measured by the width of the Ag Fermi foot; though it will change with energy. The spectra were collected at an electron takeoff angle (between surface and detector) of 85°. The angle between the beam axis and the detector is 90°.

The sampling depth, defined as three times the electron mean free path, of C 1s, O1s and F 1s photoelectrons generated by Al X-rays (1486.6 eV) at an electron takeoff angle of 90° relative to the plane of the sample (SD_{90}) are 8.7, 7.3 and 6.3 nm, respectively.[31] Note that (1) the sampling depth at an electron takeoff angle of θ (SD_θ) is equal to SD_{90}*sin(θ) and (2) the sampling depth is proportional to $(E)^m$ where E is the kinetic energy of the photoelectrons and the exponent m for many elements and compounds is very close to 0.77.[32,33] Hence, the sampling depth of Li 1s, C 1s, O 1s, F 1s, P 2p and Co 2p photoelectrons generated with Al X-rays at an electron takeoff angle of 45° are estimated to be 7.0, 6.1, 5.2, 4.5, 6.7 and 4.1 nm, respectively. On the other hand, the sampling depth of Li 1s, C1s, O 1s, F 1s, P 2p and Co 2p photoelectrons for the synchrotron X-rays with excitation energy of 2555 eV at an electron takeoff angle of 85° are 15.2, 14.1 12.9, 12.2, 14.9, and 11.7 nm, respectively.

Results and Discussion

Electrochemical performance.— The "$AlPO_4$" coating was found to improve the voltage efficiency and capacity retention when using $LiPF_6$ electrolyte, but was detrimental when cycled in the $LiClO_4$ electrolyte. As shown previously, the galvanostatic voltage profiles of lithium cells having bare and "$AlPO_4$"-coated $LiCoO_2$ electrodes revealed that the coated electrode exhibits higher capacity retention in comparison to the bare electrode upon cycling in 1 M of $LiPF_6$ in EC:DMC between 2.5–4.7 V vs. Li^+/Li with 4 hours hold at 4.7 V.[27] The galvanostatic voltage profiles of lithium cells having bare and "$AlPO_4$"-coated $LiCoO_2$ electrodes cycled in $LiPF_6$ or $LiClO_4$ between voltage limits of 2.0–4.6 V vs. Li^+/Li with 4 h hold at 4.6 V are shown in Figure 1. Clearly, the coating as well as the type of salt used during cycling has a significant effect on the degree of capacity retention and the degree of polarization. Variations

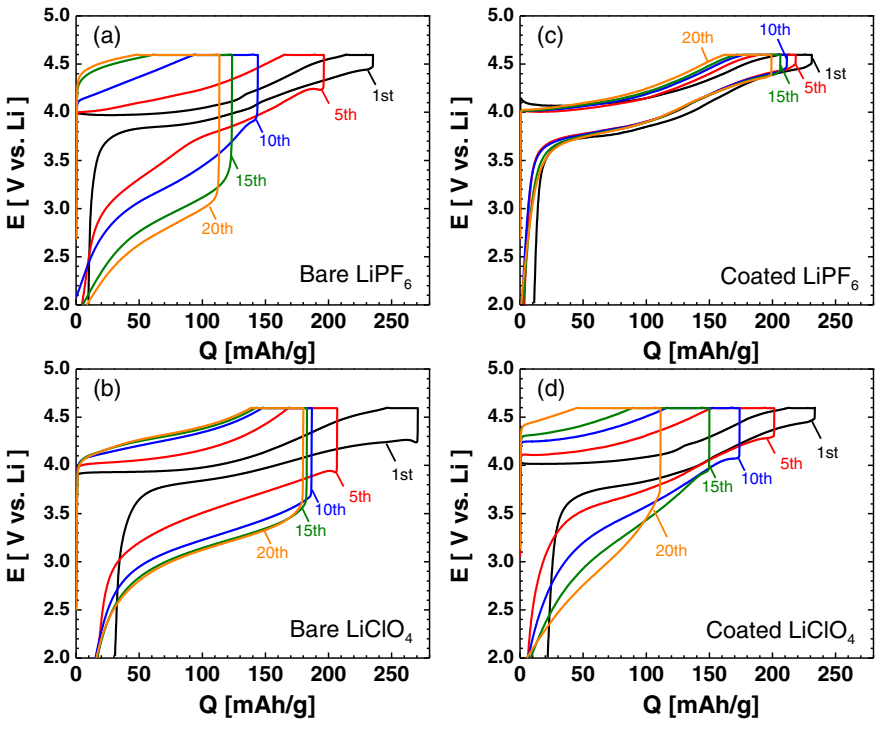

Figure 1. Voltage profiles of (a) bare $LiCoO_2$ cycled in $LiPF_6$, (b) bare $LiCoO_2$ cycled in $LiClO_4$, (c) "$AlPO_4$"-coated $LiCoO_2$ cycled in $LiPF_6$, and (d) "$AlPO_4$"-coated $LiCoO_2$ cycled in $LiClO_4$.

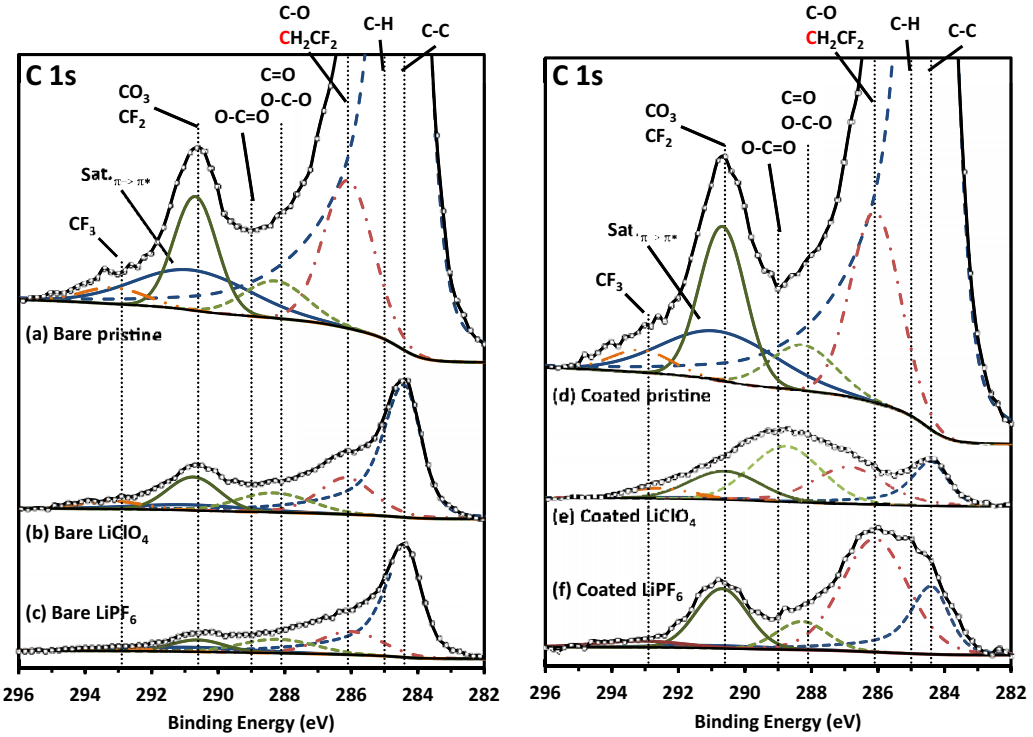

Figure 2. XPS spectra of the C 1s photoemission line for (a) pristine, bare $LiCoO_2$, (b) bare $LiCoO_2$ cycled in $LiClO_4$, (c) bare $LiCoO_2$ cycled in $LiPF_6$, (d) pristine, "$AlPO_4$"-coated $LiCoO_2$, (e) coated $LiCoO_2$ cycled in $LiClO_4$, and (f) coated $LiCoO_2$ cycled in $LiPF_6$. It should be noted that the y-axis is the same for the spectra and the spectra have simply been shifted vertically for ease of comparison. The dashed vertical lines represent binding energy values for graphitic carbon (C-C), hydrocarbon (C-H), carbon singly bound to oxygen (C-O), carbon bound to hydrogen in PVDF (CH_2CF_2), carbon doubly bound to a single oxygen atom (C=O), carbon singly bound to two oxygen atoms (O-C-O), carbon bound to two oxygen atoms through carboxylic acid type arrangement (O-C=O), carbonate (CO_3), carbon bound to two fluorine atoms in PVDF (CF_2), the π^* satellite from graphitic carbon (Sat.$_{\pi\rightarrow\pi^*}$), and carbon bound to three fluorine atoms (CF_3). These binding energy values were obtained from the referenced literature or determined via standards where noted. It should be noted that the y-axis is the same for all spectra but were shifted vertically for clarity.

in discharge capacity (mAh/g), discharge energy (Wh/kg) and energy efficiency (percent of discharge energy to charge energy) with cycle number are shown in Figure S1. The coated electrode cycled in $LiPF_6$ has the highest capacity retention. It is interesting to note that the bare electrode cycled in $LiClO_4$ has higher capacity retention than the bare electrode cycled in $LiPF_6$ or the coated electrode cycled in $LiClO_4$. Hence, the coating doesn't provide an advantage when cycling was performed in $LiClO_4$ electrolyte. The advantages of the "$AlPO_4$" coating are more dramatic when one examines the discharge energy and energy efficiency (Figure S1). The discharge energy and energy efficiency for the 20th cycle decreased in the following order: coated electrode cycled in $LiPF_6$ (≈770 Wh/kg, ≈90%), bare electrode cycled in $LiClO_4$ (≈500 Wh/kg, ≈63%), coated electrode cycled in $LiClO_4$ (≈300 Wh/kg, 56%), bare electrode cycled in $LiPF_6$ (≈300 Wh/kg, ≈54%).

It is known that structural instability can occur when $LiCoO_2$ is cycled to high cutoff voltages (>4.2 V) and can cause degradation in battery performance and capacity retention. Previously, based on synchrotron X-ray diffraction data, we were able to show that the "$AlPO_4$"-coating prevented any structural instability, even when cycling in $LiPF_6$ electrolyte to 4.7 V.[27] Therefore, we are attributing the observed reduction in capacity retention to surface chemical changes and not to lattice instability when comparing the coated electrode cycled in $LiPF_6$ versus the coated electrode cycled in $LiClO_4$.

Scanning electron or transmission electron microscopy micrographs of the cycled active material to look for cracks or degradation of the primary particles of $LiCoO_2$ were not taken. Though we believe a mechanical degradation study to be of interest, our extensive literature search suggested that $LiClO_4$ is commonly used as a model electrolyte salt because it does not mechanically damage the active particles. A study by Ozawa, Yazami, and Fultz[34i]ndicated that $LiClO_4$ caused some measure of lithium re-intercalation, but no mechanical damage, when the cathode material was thermally aged for several weeks. Aurbach et al.[35] found that Fe dissolution in $LiClO_4$ was negligible even at elevated temperatures due to the lack of acidic contaminants and that Co dissolution occurred in $LiPF_6$ based electrolytes. Hereafter, we describe the surface chemical changes evolved after cycling in $LiClO_4$ and $LiPF_6$ as determined by XPS.

XPS/Surface chemistry.— All cycled electrodes were examined in the discharged state. A comparison of survey spectra of various electrodes is shown in Figure S2. The C 1s, O 1s, Co 2p and F 1s spectra are shown in Figures 2–5, respectively. The Li 1s, P 2p, Cl 2p and Al 2p spectra are shown in Figures S3–S6, respectively. The concentrations based on these spectra are provided in Table I. The compositions of the near surface region for the pristine bare and coated electrodes are dominated by carbon, fluorine and then oxygen. The binding energy, full width-at-half-maximum (FWHM) and concentrations (in atomic percent) of various elements for each proposed chemical state are summarized in Table SI. The depth profile spectra of the O 1s, Co 2p, C 1s and F 1s regions are shown in Figures S7–S10, respectively, with concentrations based on these spectra are shown in Figure S11. Hereafter, we discuss the results for each element and correlate surface chemistry with electrochemical performance characteristics.

C 1s region.— The surface film developed in coated electrodes were found to be thicker with more oxygenated nature compared to that developed in bare electrode in both electrolytes based on the changes in C 1s intensity and binding energy. The C 1s photoemission spectra of pristine bare (Figure 2a) and pristine coated (Figure 2d) electrodes are dominated by the contributions from carbon black and PVDF. Various carbon chemistries are highlighted by

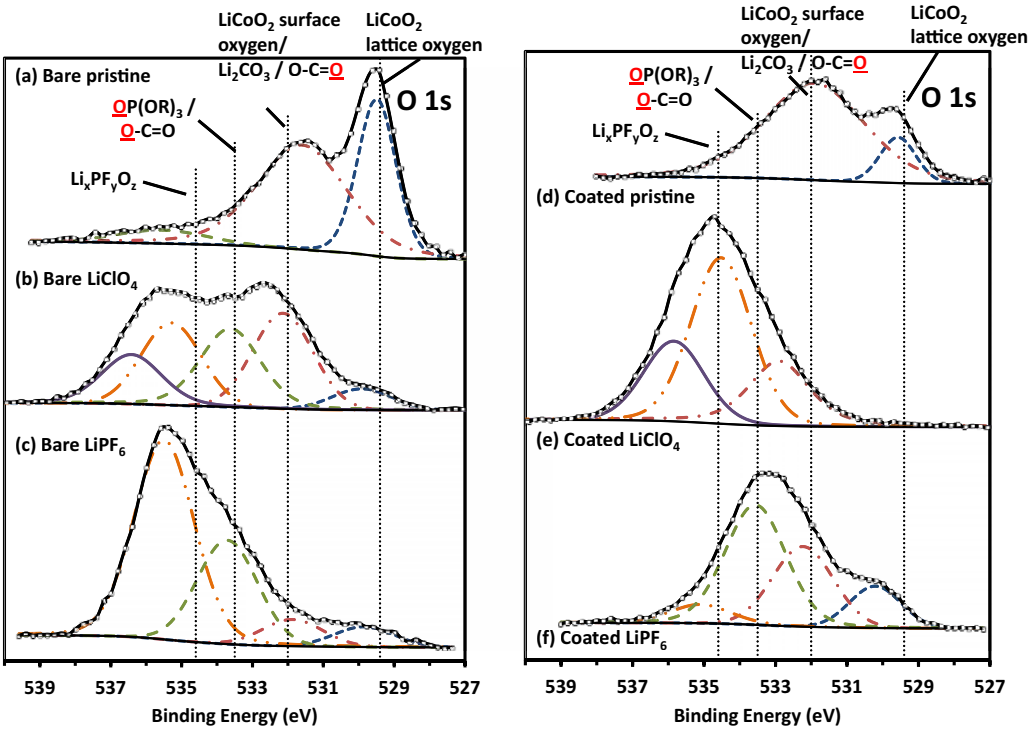

Figure 3. XPS spectra of the O 1s photoemission line for (a) pristine, bare $LiCoO_2$, (b) bare $LiCoO_2$ cycled in $LiClO_4$, (c) bare $LiCoO_2$ cycled in $LiPF_6$, (d) pristine, "$AlPO_4$"-coated $LiCoO_2$, (e) coated $LiCoO_2$ cycled in $LiClO_4$, and (f) coated $LiCoO_2$ cycled in $LiPF_6$. The dashed vertical lines represent binding energy values for lattice oxygen ($LiCoO_2$ lattice oxygen), oxygen present in lithium carbonate (Li_2CO_3), oxygen doubly bound to carbon in a carboxylic acid arrangement (O-C=O*), oxygen bound to phosphorus (O*P(OR)$_3$), oxygen singly bound to carbon in a carboxylic acid arrangement (O*-C=O), and oxygen in a fluorine based compound from $LiPF_6$ degradation ($Li_xPF_yO_z$). It should be noted that the y-axis is the same for all spectra but were shifted vertically for clarity.

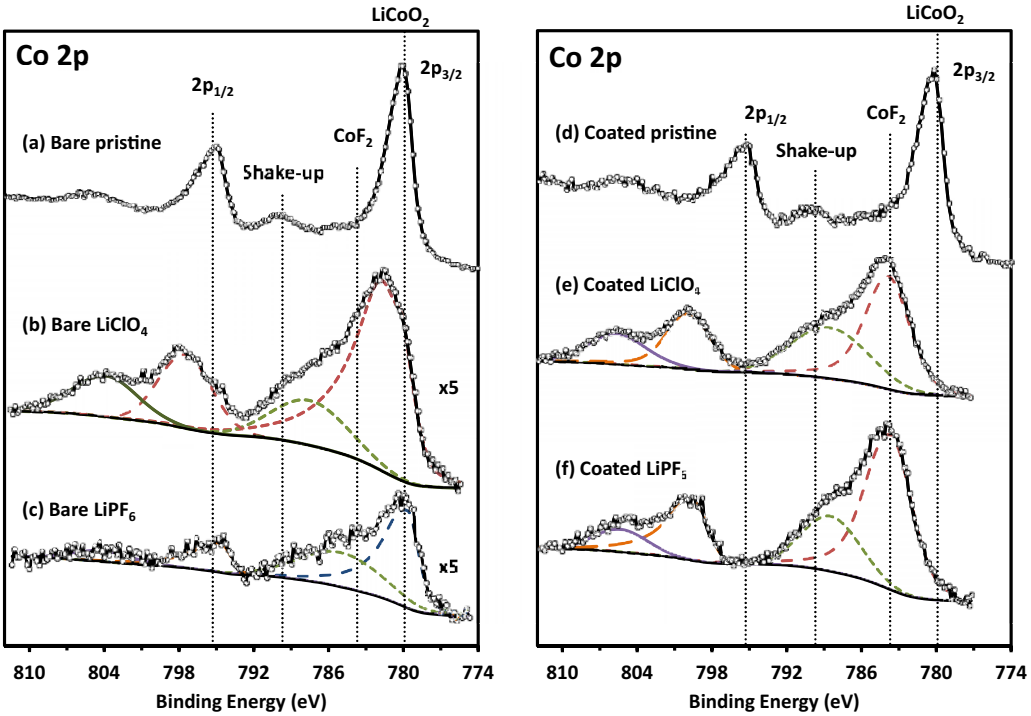

Figure 4. XPS spectra of the Co 2p photoemission line for (a) pristine, bare $LiCoO_2$, (b) bare $LiCoO_2$ cycled in $LiClO_4$ (where the signal is multiplied by 5 for ease of viewing), (c) bare $LiCoO_2$ cycled in $LiPF_6$ (where the signal is multiplied by 5 for ease of viewing), (d) pristine, "$AlPO_4$"-coated $LiCoO_2$, (e) coated $LiCoO_2$ cycled in $LiClO_4$, and (f) coated $LiCoO_2$ cycled in $LiPF_6$. The dashed vertical lines represent binding energy values for lattice cobalt ($LiCoO_2$ $2p_{3/2}$ and $2p_{1/2}$), cobalt fluoride (CoF_2) and the Co $2p_{3/2}$ satellite shake-up (Shake-up). It should be noted that the y-axis is the same for all spectra but were shifted vertically for clarity. However, the spectra for the bare electrode cycled in $LiClO_4$ (b) and in $LiPF_6$ (c) were scaled by a factor of 5.

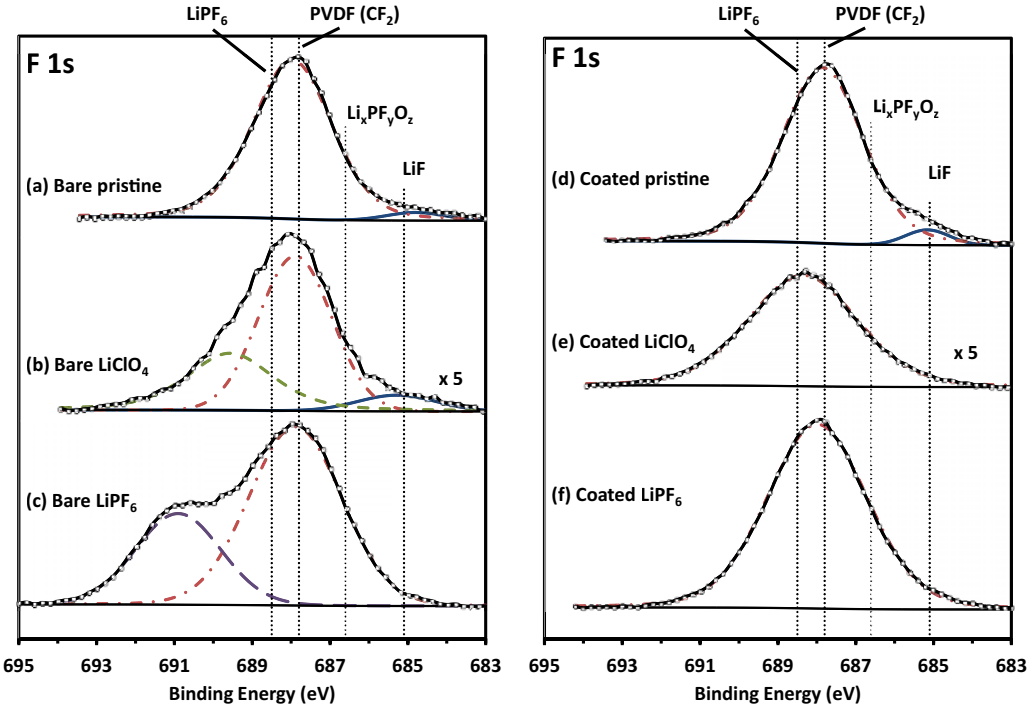

Figure 5. XPS spectra of the F 1s photoemission line for (a) pristine, bare $LiCoO_2$, (b) bare $LiCoO_2$ cycled in $LiClO_4$ (where the signal is multiplied by 5 for ease of viewing), (c) bare $LiCoO_2$ cycled in $LiPF_6$, (d) pristine, "$AlPO_4$"-coated $LiCoO_2$, (e) coated $LiCoO_2$ cycled in $LiClO_4$ (where the signal is multiplied by 5 for ease of viewing), and (f) coated $LiCoO_2$ cycled in $LiPF_6$. The dashed vertical lines represent binding energy values for lithium fluoride (LiF), $LiPF_6$ degradation products ($Li_xPF_yO_z$), PVDF (CF_2), and the $LiPF_6$ salt. It should be noted that the y-axis is the same for all spectra were shifted vertically for clarity. However, the spectra for the bare (b) and the coated (e) electrode cycled in $LiClO_4$ were by a factor of 5.

the dashed lines (Figure 2) as follows: carbon black (284.4 eV), hydrocarbon (285.0 eV), $C^*H_2CF_2$ (285.9 eV), C-O (≈286.5), C=O or O-C-O (≈288 eV), O-C=O (≈289 eV), $ROCO_2R$ or Li_2CO_3 (≈290.2 eV), $CH_2C^*F_2$ (290.6 eV), and $-CF_3$ (≈293.5 eV). As previously described, reference spectra of Super P carbon black, PVDF, and a composite electrode of 50 wt% PVDF and 50 wt% Super P carbon black were used as a guide to deconvolute the spectra of pristine composite electrodes.[27] This procedure resulted in satisfactory fits for all of the cycled electrodes, except for the coated electrode cycled in $LiClO_4$. In this case, the binding energies for all components were allowed to vary except those for carbon black, where the binding energy separation and FWHM for the main peak and its satellite were constrained to the reference electrode values. The additional small components, which we assign to -CHF and $-CF_3$, were also observed for a powder sample of PVDF and we believe are at least, in part, due to sample damage by the X-rays.

As can be seen from the data in Figure 2 and Table SI, the concentration of carbon black (≈284.4 eV) for the bare and coated electrodes cycled in $LiPF_6$ and $LiClO_4$ decreased significantly relative to concentrations for the pristine electrodes, which can be related to the buildup of surface films on the electrode surfaces. Both bare electrodes (cycled in $LiPF_6$ and $LiClO_4$) have a larger contribution of the carbon black signal compared to their coated counterparts. The sub-peaks associated with the CH_2-CF_2 chemistries (≈286.1 and 290.6 eV) for the cycled electrodes have concentrations close to those observed for the pristine electrodes except in the case of the bare electrode cycled in $LiPF_6$, which has significantly lower contributions. Furthermore, the broader nature of these sub-peaks for the cycled electrodes relative to the pristine electrodes may indicate the presence of multiple chemistries and therefore these sub-peaks may not only be associated with -CH_2-CF_2- from PVDF, but also with C-O and Li_2CO_3 type of species, respectively. For instance, Dedryvère et al.[36] assigned a peak at 286.0 eV as oligomer species of poly(ethylene oxide) type, $(CH_2CH_2O)_n$, resulting from the decomposition of ethylene carbonate in the electrolyte. Another investigation by the same group[37] assigned peaks at 286.4 and 286.7 eV to the carbon singly bound to oxygen in lithium ethyl carbonate ($CH_3C^*H_2$-O-CO_2Li) and lithium methyl carbonate (C^*H_3-O-CO_2Li), respectively. The third sub-peak at ≈288.3 eV can be assigned to a carbon doubly bound to oxygen or singly bound to two oxygen atoms, or to fluorinated alkyl carbonate (R-CF_2-C^*H_2-O-CO_2-R).[38] The third sub-peak for the coated electrode cycled in $LiClO_4$ is again at a higher binding energy (≈288.8 eV), which can be related to a carboxylic chemistry. The final sub-peak at ≈293.1 eV is assigned to CF_3 chemistries. This sub-peak contribution is relatively weak for all electrodes, though the bare and coated electrodes cycled in

Table I. Summary of elemental concentrations (in atomic percent) as determined from XPS multiplex spectra.

Sample	At. % Li	At. % C	At. % O	At. % F	At. % Co	At. % Al	At. % P	At. % Cl
Bare pristine	2.0	68.1	8.4	19.1	2.3	N/A	N/A	N/A
Coated pristine	2.2	65.7	7.2	22.5	1.0	0.8	0.6	N/A
Bare $LiPF_6$	24.9	11.1	12.9	43.8	0.6	1.7	5.1	N/A
Coated $LiPF_6$	26.4	17.2	12.8	36.9	2.4	0.5	3.9	N/A
Bare $LiClO_4$	0.0	43.7	31.3	16.1	3.9	4.7	N/A	0.3
Coated $LiClO_4$	0.0	30.8	41.3	12.2	4.8	9.3	1.2	0.5

$LiClO_4$ have larger contributions, suggesting a reaction involving the PVDF binder. The above assignments are supported with assignments from the other XPS regions in the forthcoming discussions.

A relative estimate for the thickness of the surface films can be made based on the reduction of the C 1s intensity for carbon black in the cycled electrodes relative to that in the pristine electrodes. It is well known that a thin over layer with a uniform thickness will attenuate the intensity of the photoelectrons from the underlayer following the relationship

$$I/I_0 = e^{-d/\lambda_c * sin\theta}$$

where d is the thickness of the over layer, λ_c is the mean free path of the photoelectrons, and θ is the electron takeoff angle relative to the plane of the sample which is 45° in this experiment with Al X-rays.[39,40] For C 1s photoelectrons using Al X-rays, λ_c is ≈2.9 nm[31] and, hence, the overlayer film thicknesses are estimated to be ≈ 4.2 and 1.6 nm for the bare electrode cycled in $LiPF_6$ and $LiClO_4$, respectively, and ≈ 5.3 and 4.4 nm for the coated electrode cycled in $LiPF_6$ and $LiClO_4$, respectively. It should be noted, and stressed, that a uniform thickness or composition may not be the case for the cycled electrodes. Therefore, these estimates are a crude measure for film thickness and may be compared on a relative basis. It should also be noted that XPS measurements offer a non-destructive means of measuring the film thickness without interfering with the chemical integrity of the film.

O 1s region.— The O 1s photoemission spectra for the pristine bare (Figure 3a) and coated (Figure 3d) electrodes display prominent contributions from $LiCoO_2$ lattice oxygen (O^{2-}), surface oxygen (O^-), and Li_3PO_4 at 531.5 eV based on our reference (in the case of the coated electrode) in good agreement with previously reported results.[27,28] The lattice oxygen at ≈529.5 eV, the surface oxygen species O-C = O* and Li_2CO_3 collectively at ≈532.1 eV, the O*P(OR)$_3$ and O*-C = O species at ≈533.5 eV and $Li_xPF_yO_z$ at ≈534.6 eV are identified by the dashed lines (Figure 3).

The sub-peak at 529.8 eV for the bare electrode cycled in $LiPF_6$ is close to that observed for our $Co(OH)_2$ reference at 530.1 eV indicating that surface Co is present in the form of $Co(OH)_2$ in agreement with the assignment based on the Co 2p region. On the other hand, the sub-peak at 529.9 eV for the bare electrode cycled in $LiClO_4$ is similar to that observed for our CoO reference at 529.9 eV indicating that surface Co is present in the form of CoO in agreement with the assignment based on the Co 2p region. The differentiation between $Co(OH)_2$ and CoO was based mainly on the Co 2p region as will be discussed later in the text. The sub-peak at 530.2 eV for the coated electrode cycled in $LiPF_6$, cannot be attributed to $LiCoO_2$, CoO or $Co(OH)_2$ as the Co 2p region confirmed the absence of these phases. Recent work by the Edström group[41,42] has indicated a binding energy of 530.3 eV is indicative of a Li_4SiO_4 and work by Ramana et al. assigns a binding energy of 530.1 eV to $LiMn_2O_4$[43] and 530.9 eV to $LiFe_2P_3O_{10}$.[44] Early work by Morgan et al. suggests a variety of pyrophosphates result in a binding energy of approximately 530.2 eV.[45] Clearly the literature indicates that this sub-peak is associated with oxygen as a polyanion. It is to be noted that such a low binding energy component is absent in the case of the coated electrode cycled in $LiClO_4$.

The O1s component located between 531.6 – 532.2 eV can be attributed to the surface oxygen of $LiCoO_2$ and oxygen in Li_2CO_3. Contributions at ≈531.6 eV (pristine bare electrode) and ≈531.9 eV (pristine coated electrode) are significantly reduced upon cycling in $LiPF_6$. This contribution, however, is significantly increased upon cycling the bare electrode in $LiClO_4$, but is absent in the case of the coated electrode cycled in $LiClO_4$. The binding energy of this component increased upon cycling from 531.6 to 531.9 eV (bare electrode in $LiPF_6$), 531.6 to 532.1 eV (bare electrode in $LiClO_4$), and 531.9 to 532.2 eV (coated electrode in $LiPF_6$) indicating that this subpeak is dominated by contributions from carbonate chemistry and/or oxygen doubly bonded to carbon (C = O) upon cycling. The sub-peak at ≈533.7 eV, which can be associated with oxygen singly bound to carbon (RO*-CO-O*R) in carbonate, emerged at a moderate level upon cycling bare and coated electrodes in $LiPF_6$ and bare electrode in $LiClO_4$, which has the highest contribution of this component.

The high binding energy sub-peak at ≈535.5 eV, seen in the pristine bare electrode, the bare electrode cycled in $LiClO_4$, and the bare electrode cycled in $LiPF_6$, was not observed in any of our reference compounds. This sub-peak has been reported to be the result of carbonate impurities on the surface of the $LiCoO_2$ particles.[46] This contribution emerged at significant levels upon cycling bare electrodes in $LiPF_6$ and $LiClO_4$. A weak contribution (≈1 atomic %) with a slightly lower binding energy (535.1 eV) was observed for the coated electrode cycled in $LiPF_6$. Also, a sub-peak is observed at ≈536.4 eV for the bare electrode cycled in $LiClO_4$ and a sub-peak is observed at ≈535.8 eV for the coated electrode cycled in $LiClO_4$, which were not present in any of the reference materials we used for calibration purposes. For the coated electrode cycled in $LiClO_4$, a unique sub-peak at ≈532.9 eV emerged, which can be related to oxygen doubly bound to carbon. Another unique sub-peak at 534.5 eV also emerged, which can be related to oxygen singly bound to carbon. Due to the observed high binding energies, these components are thought to be the result of differential charging as a result of low electrical conductivity of the electrode sample after cycling. This further complicates not only the O 1s assignments and differentiation of the peaks associated with $Li_xPF_yO_z$ and alkyl carbonates, but the C 1s assignments as well and can only be speculated currently.

The lack of a contribution from the $LiCoO_2$ lattice oxygen sub-peak for the bare electrode cycled in $LiPF_6$ in this study, which was not the case in our previous study,[27] indicates that the surface film being formed is thicker in the current investigation. The formation of a thicker film could be the result of cycling between 2.0–4.6 V in the current investigation versus 2.5–4.7 V in the previous investigation, as the electrolyte is more likely to break down while discharging to 2.0 V. As previously reported for the coated electrode cycled in $LiPF_6$, the oxygen species were considered to be associated with the formation of Co-Al-O-F and $PF_x(OH)_y$ species. On the other hand, the oxygen species for the bare electrode cycled in $LiPF_6$ included significant contributions from lattice oxygen, Li_2CO_3, O-C=O, and $Li_xPF_yO_z$. As will be discussed later, based on the binding energy of the Cl 2p line and its concentration, none of the oxygen signal for the electrodes cycled in $LiClO_4$ can be attributed to the salt. The electrodes cycled in $LiClO_4$ have contributions from higher binding energy sub-peaks. This would suggest that the salt is decomposing and reacting with the solvent material, forming insoluble reaction products that are on the surface of the electrode or become part of the surface film. The bare electrode cycled in $LiPF_6$ has a larger contribution from the sub-peak at ≈535.4 eV, which is considered to play a role in the performance profile. The coated electrode cycled in $LiClO_4$ has the highest concentration of high binding energy oxygen chemistries, indicating a thicker resistive surface film that is forming on the surface and accounting for the poor electrochemical performance.

The presence of the higher binding energy sub-peaks in the O 1s region at ≈536 eV observed for the electrodes cycled in $LiClO_4$ could indicate the formation of ether-based solid products, which result from the breakdown of the electrolyte.[47–50] These species are resistive as illustrated by the differential charging observed in the hard X-ray data, which will be discussed later in the text. The large contribution of the oxygen sub-peak at 535.5 eV for the bare electrode cycled in $LiPF_6$ compared to the coated electrode cycled in $LiPF_6$ suggests oxygen interaction with fluorine, possibly as suggested by Veith et al.,[47] but certainly the formation of more covalent and/or polymeric material than in the case of the coated electrode.[48–50]

Co 2p region.— Cobalt fluoride was found to dominate the cobalt chemistry in coated electrodes cycled in both electrolytes but not in bare electrodes. The Co 2p spectra for the pristine bare (Figure 4a) and coated (Figure 4d) electrodes, with the Co $2p_{3/2}$ peak at ≈780 eV and the satellite at approximately +10 eV, are characteristic of $LiCoO_2$ and $LiAl_yCo_{(1-y)}O_2$, respectively. The cobalt signal for the bare electrode cycled in $LiPF_6$ at 779.8 eV is very weak and, therefore, resulting in a poorly developed satellite structure at ≈+6.1 eV.

These values compare well with our values for $Co(OH)_2$ (Co $2p_{3/2}$ at 779.8 eV) with a satellite structure at 6.1 eV higher indicating that the majority of surface Co is present in the form of $Co(OH)_2$. The $Co(OH)_2$ chemistry is also supported by results based on the O 1s region. For the bare electrode cycled in $LiClO_4$, the Co $2p_{3/2}$ line has a binding energy of 780.3 eV with a satellite structure at approximately +7 eV. These values compare well to our values for the CoO reference (Co $2p_{3/2}$ at 780.0 eV and satellite contribution at +7 eV) indicating that a large portion of surface Co is present in the form of CoO. This assignment is also supported by results based on the O 1s region. However, the presence of a modest amount of CoF_2 and/or oxyfluoride cannot be ruled out as the peak is slightly shifted to higher binding energy relative to that for CoO. The presence of the CoF_2 and/or oxyfluoride is confirmed based on synchrotron XPS data as will be demonstrated later in the text. The spectrum for the coated electrode cycled in $LiPF_6$ with the $2p_{3/2}$ peak at ≈783.7 eV and a satellite separation of ≈+5 eV is consistent with the reference spectrum of CoF_2 indicating the formation of cobalt fluoride in agreement with previous results.[27] The spectrum for the coated electrode cycled in $LiClO_4$ with a Co $2p_{3/2}$ sub-peak at ≈783.9 eV also indicates the formation of CoF_2.

The Co concentrations for the electrodes cycled in $LiClO_4$ are higher than those for the electrodes cycled in $LiPF_6$ (Table S1). It is noted that the sampling depth for the Co 2p electrons is 4.1 nm, which is smaller than or comparable to the overlayer film thickness as determined based on the C 1s region except in the case of the bare electrode cycled in $LiClO_4$ where it is greater than the overlayer thickness. Hence, the Co signal is from Co residing in the overlayer film except in the case of the bare electrode cycled in $LiClO_4$ where the Co signal can have an additional contribution from Co residing below the overlayer film. Therefore, Co dissolution may occur more frequently in $LiClO_4$ cycled electrodes, which then results in Co products being deposited in the overlayer film.[3]

As reported previously,[27] the formation of CoF_2 in the case of the $LiPF_6$ electrolyte can be due to a reaction between $LiCo_{(1-y)}Al_yO_2$ and/or $LiCoO_2$ with HF present as an impurity in the electrolyte. However, in the case of the $LiClO_4$ electrolyte, the only source of F is the PVDF binder, which can produce HF as a result of a dehydrofluorination reaction as reported previously.[25,26] The reaction mechanism, therefore, could be similar for both the $LiPF_6$ and $LiClO_4$ electrolytes but the source of HF is different. In one case, it is the HF impurity in $LiPF_6$ and, in the other case, dehydrofluorination of the PVDF binder.

F 1s region.— The F 1s spectra from the pristine electrodes (Figures 5a and 5d) display mainly a single peak at ≈687.8 eV, which corresponds to fluorine chemistry from PVDF. A weak component with binding energy of ≈685 eV is also observed and can be related to the presence of LiF. The origin of LiF was attributed previously to a dehydrofluorination reaction of PVDF generating HF, which then reacts with $LiCoO_2$ or Li_2CO_3 present on the surfaces of the $LiCoO_2$ particles to form LiF.[25] Upon cycling the bare electrode in $LiPF_6$, the majority of the F signal arises from species at 687.9 eV, associated with PVDF, $LiPF_6$ and its degradation products. However, a high binding energy peak (≈690.9 eV) is also present. This high binding energy was reported in recent Li-air work and was assigned to highly ionic species formed with the addition of organic groups promoted by organo-lithium.[47] The high binding energy species, however, could also be the result of highly resistive species that is experiencing differential charging. For the coated electrode cycled in $LiPF_6$, a single broad peak is observed at ≈688.0 eV, which is assigned to PVDF, $LiPF_6$ and its degradation products.

For the $LiClO_4$-cycled electrodes, the fluorine contribution was limited to PVDF and the relative intensity of the F 1s signal reflects this (the signal in Figure 5 is multiplied by 5 for clarity). For both the bare and coated electrodes cycled in $LiClO_4$, the F 1s region consists of a major contribution with binding energy of ≈688.0 eV, which can be associated with PVDF and AlF_3 (with F 1s binding energy of 687.4 eV from our AlF_3 reference). Al comes from the current collector in the case of the bare electrode, but also from the coating in the case of the coated electrode. For the bare electrode cycled in $LiClO_4$, a component with binding energy at 685.3 eV, which can be related to LiF, and a high binding energy component at 689.6 eV, which could be associated with a highly ionic species within organic material as mentioned previously or differential charging, were also present.

Based on our CoF_2 reference, a subpeak which corresponds to the CoF_2 chemistry is expected at ≈686.0 eV in the F 1s region. However, due to the relatively large concentration of F from PDVF as well as $LiPF_6$ and its degradation products in the case of coated electrode cycled in $LiPF_6$, the subpeak associated with CoF_2 chemistry is not clearly resolvable. However, the assignment for the CoF_2 chemistry was clearly confirmed based on the Co 2p photoemission region as discussed earlier.

Al 2p region.— The Al 2p spectrum for the pristine coated electrode (Figure S6) displays a peak at ≈73.7 eV that is associated with $LiAl_yCo_{(1-y)}O_2$, while that for the coated electrode cycled in $LiPF_6$ displays a peak at ≈76.4 eV that is associated with Al-F-O and/or AlF_3 species. As expected, no Al contribution is observed for the pristine bare electrode. The Al 2p spectrum for the bare electrode cycled in $LiPF_6$ consists of a single peak at 76.9 eV, which is associated with Al-F-O and/or AlF_3 from the interaction of the current collector with the $LiPF_6$ electrolyte and/or PVDF. The Al spectrum for the bare electrode cycled in $LiClO_4$ consists of two sub-peaks at 76.1 eV and 78.2 eV, which can be associated with Al-F-O and/or AlF_3. The Al 2p spectrum for the coated electrode cycled in $LiClO_4$, however, consists of a relatively large intensity sub-peak at ≈77.4 eV that is considered to be associated with AlF_3 and/or an Al-F-O oxyfluoride chemistries. The higher binding energies observed for the bare electrode cycled in $LiPF_6$ and $LiClO_4$ relative to that observed for our AlF_3 reference (76.7 eV) suggest a resistive film that is differentially charging. It should be noted that the atomic concentrations for aluminum are significantly higher for the $LiClO_4$ cycled electrodes than for the $LiPF_6$ cycled electrodes and the pristine electrodes. Therefore, since the $LiClO_4$ cycled electrodes surfaces have no visible spots from the current collector, which could contribute to the Al spectrum, the origin of the Al signal would be due to Al dissolution and re-deposition onto/into the cathode surface during cycling, as aluminum is known to be subject to corrosion under high potentials and electrolyte compositions.[51–53] This could be due to the detachment of the active material at the current collector interface and the subsequent Al dissolution into the electrolyte and its re-deposition on the electrode surface. Similar corrosion products of the Al current collector were reported to occur after cycling in $LiPF_6$ in PC:DEC and EC:DMC electrolytes.[51]

Synchrotron based XPS.— In an effort to examine the depth distribution of the respective surface films and the thickness of the metal fluoride phases, the electrodes were also inspected using monochromatic synchrotron X-rays with energy of 2555 eV. The O 1s photoemission spectra (Figure S12) are similar to spectra obtained using our conventional in-house spectrometer (Figure 3) with one very noticeable exception. Only electrodes cycled in $LiClO_4$ exhibit intense high binding energy peaks beyond 536 eV. The F 1s spectra (Figure S13) are also similar to the in-house spectra (Figure 5), except for the high binding energy peaks (∼693 eV), which appeared in electrodes cycled in $LiClO_4$. High binding energy peaks were also observed in the Al 2p and Al 2s spectra (not shown) and were all shifted by similar amount as those of the F and O high binding energy peaks. We believe that these high binding energy peaks associated with O, F and Al are the result of differential charging. Thus, the highly resistive species appear to contain Al, O, and F. Clearly, the films formed on the surfaces of the electrodes cycled in $LiClO_4$ are more resistive in nature than the films formed on the surfaces of the electrodes cycled in $LiPF_6$, regardless of the coating. Therefore, we speculate that these species could be due to dissolution of the Al current collector and its redeposition onto/into the electrode surface. Differential charging occurs less frequently with spectrometers employing conventional nonmonochromatic Al or Mg X-rays relative to spectrometers employing monochromatic synchrotron radiation. In the case of conventional spectrometers, the secondary electrons,

generated by the X-rays passing through the window of the source, tend to neutralize the sample surface.

Synchrotron based XPS helps to reveal the thickness of the CoF_2 formed in the coated electrode cycled in $LiPF_6$. The Co 2p spectrum (Figure S14) for the bare $LiCoO_2$ electrode cycled in $LiPF_6$ is consistent with conventional data showing no contribution from CoF_2. The Co 2p spectrum for the bare electrode cycled in $LiClO_4$, displays contributions from lattice $LiCoO_2$ as well as CoF_2. However, the Co 2p spectrum for the coated $LiCoO_2$ electrode cycled in $LiPF_6$ displays a contribution from $LiCoO_2$ in addition to the CoF_2 contribution. Since CoF_2 is the only chemistry observed in the case of conventional data, it suggests the depth of the region that contains CoF_2 for the coated $LiCoO_2$ electrode cycled in $LiPF_6$ to be greater than 4 but less than 11 nm. The formation of CoF_2 also occurs in the case of the electrodes cycled in $LiClO_4$ as the surface doesn't contain enough chlorine to account for all of the highly oxidized Co. The extent of the formation of CoF_2 is greater in the case of the coated $LiCoO_2$ electrode cycled in $LiClO_4$ relative to the bare electrode cycled in $LiClO_4$. The CoF_2 peak was also observed in conventional data for both the bare and coated $LiCoO_2$ electrodes cycled in $LiClO_4$ and cannot be attributed to differential charging. In this case, the formation of CoF_2 suggests an interaction with the PVDF binder since it is the only source of F. Such an interaction could lead to degradation of PVDF and the loss of electrical connectivity between particles and be responsible for the poor performance.

Conclusions

Our previous work based on high resolution synchrotron X-ray diffraction data,[27] showed that the addition of the "$AlPO_4$"-coating prevented lattice instability when cycling in $LiPF_6$ electrolyte even at higher voltages (4.7 V). Based on surface analysis by XPS and the XRD results, we proposed that the coating offers protection against corrosion by HF, in addition to lattice stability of the coated $LiCoO_2$ in the cathode. Based on voltage-capacity profiles in Figure 1, the observed trends in discharge energy and energy efficiency after 20 cycles are as follows: "$AlPO_4$"-coated electrode in $LiPF_6$ (≈770 Wh/kg, ≈90%), bare electrode cycled in $LiClO_4$ (≈500 Wh/kg, ≈63%), "$AlPO_4$"-coated electrode cycled in $LiClO_4$ (≈300 Wh/kg, 56%), bare electrode cycled in $LiPF_6$ (≈300 Wh/kg, ≈54%). Chemical analysis via XPS in the current investigation revealed several interesting results. The electrodes cycled in $LiClO_4$ showed CoF_2 formation in the Co 2p photoemission region (Figure 4). The only source of fluorine for these electrodes is the PVDF binder, suggesting dehydrofluorination or leaching of the F from the material. Also, Al was detected in the surface films for the bare electrodes. The Al concentrations are significantly higher for the electrodes cycled in the $LiClO_4$ electrolyte. This suggests that there is corrosion of the current collector and then redeposition from the electrolyte onto/into the surface film. The corrosion of the current collector has been shown previously,[51–53] but the degree of corrosion and exactly what variable has caused the corrosion is currently unclear. An estimation of the film thickness was made based on attenuation of the carbon black intensity for the cycled electrodes relative to that of the corresponding pristine electrodes. Sputter depth profiling with energetic Ar-ions (4 keV) provided some information (Figures S7–S10), but information from the C 1s region is of limited use as the bombardment of carbon films is known to cause some chemical changes to the carbon morphologies.[54,55] Additionally, differential charging observed in the synchrotron-based XPS studies support the electrically resistive nature of the Al oxyfluoride (Al-O-F) formed during cycling in the $LiClO_4$ electrolyte.

The "$AlPO_4$" coating was found to improve the voltage efficiency and capacity retention when using the $LiPF_6$ electrolyte, but was detrimental when using the $LiClO_4$ electrolyte. This indicates that the enhanced cycling performance with surface coating is only realized when cycling in $LiPF_6$, suggesting that while the coating material may prevent HF corrosion of the active material, the electrolyte composition also plays a key role in cell performance. XPS reveals that the "$AlPO_4$" coating promotes the formation of metal fluoride (e.g. CoF_2 and Al-O-F) in both electrolytes. The source of fluorine in the coated $LiCoO_2$ electrode cycled in $LiPF_6$ is largely attributed to the $LiPF_6$ salt whereas the source of fluorine in the coated $LiCoO_2$ electrode cycled in $LiClO_4$ is the binder PVDF. Furthermore, the data appear to indicate that the surface film formed on the bare electrodes is thinner than the surface film formed on the coated $LiCoO_2$ electrodes, with the film formed on the bare electrode cycled in $LiClO_4$ being the thinnest (≈ 1.6 nm) and the film formed on the coated $LiCoO_2$ electrode cycled in $LiPF_6$ being the thickest (≈ 5.3 nm). We stress that these are crude estimates based solely on the assumptions of a consistent photoelectron mean free path across chemistries and that these estimates are to aid the reader in addressing the questions of film thickness on a relative basis. Our study suggests that the working mechanism of "$AlPO_4$" coating is the formation of stable metal fluoride and/or Co/Al oxyfluoride surface film via reactions between the surface coating and the F source from the electrolyte (e.g., HF impurity in the $LiPF_6$ electrolyte). When the F source from the electrolyte is removed such as in the case of $LiClO_4$, the coating no longer works positively, but appears to mainly extract the fluorine from the PVDF binder causing degradation of the electrode. The fluorine source from PVDF is likely to be also HF, as a result of dehydrofluorination reaction as discussed earlier in the text.[25,26]

Acknowledgment

This work was supported in part by the MRSEC Program of the National Science Foundation under award number DMR-0819762 and the Assistant Secretary for Energy Efficiency and Renewable Energy, Office of FreedomCAR and Vehicle Technologies of the U. S. Department of Energy under contract no. DE-AC03-76SF00098 with the Lawrence Berkeley National Laboratory. The synchrotron XPS experiment was conducted on beamline X24A at the National Synchrotron Light Source of Brookhaven National Laboratory, which is supported by the U.S. Department of Energy, Office of Basic Energy Sciences, under contract no. DE-AC02-98CH10886.

References

1. J. B. Goodenough and M. Koichi, U. K. A. E. Authority, Editor. **429/104**, H01M 4/36 (1980).
2. K. Mizushima, P. C. Jones, P. J. Wiseman, and J. B. Goodenough, *Materials Research Bulletin*, **15**, 783 (1980).
3. G. G. Amatucci, J. M. Tarascon, and L. C. Klein, *Solid State Ionics*, **83**, 167 (1996).
4. D. Aurbach, *Journal of Power Sources*, **89**, 206 (2000).
5. H. Wang, Y. I. Jang, B. Huang, and D. R. Sadoway, *J. Electrochem. Soc.*, **146**, 473 (1999).
6. N. Pereira, J. F. Al-Sharab, F. Cosandey, F. Badway, and G. G. Amatucci, *J. Electrochem. Soc.*, **155**, A831 (2008).
7. Y. J. Kim, J. Cho, T.-J. Kim, and B. Park, *J. Electrochem. Soc.*, **150**, A1723 (2003).
8. S. Oh, J. K. Lee, D. Byun, W. I. Cho, and B. Won Cho, *Journal of Power Sources*, **132**, 249 (2004).
9. J. Cho et al., *Journal of Power Sources*, **146**, 58 (2005).
10. Z. Yang, W. Yang, D. G. Evans, G. Li, and Y. Zhao, *Electrochemistry Communications*, **10**, 1136 (2008).
11. C. M. Julien, A. Mauger, K. Zaghib, and H. Groult, *Inorganics*, **2**, 132 (2014).
12. J. Cho, Y. J. Kim, and B. Park, *J. Electrochem. Soc.*, **148**, A1110 (2001).
13. G. T.-K. Fey et al., *Journal of Power Sources*, **132**, 172 (2004).
14. Z. Chen and J. R. Dahn, *Electrochem. Solid-State Lett.*, **5**, A213 (2002).
15. Z. Chen and J. R. Dahn, *Electrochem. Solid-State Lett.*, **7**, A11 (2004).
16. Y. Bai, N. Liu, J. Liu, Z. Wang, and L. Chen, *Electrochem. Solid-State Lett.*, **9**, A552 (2006).
17. B. J. Hwang, C. Y. Chen, M. Y. Cheng, R. Santhanam, and K. Ragavendran, *Journal of Power Sources*, **195**, 4255 (2010).
18. L. Dahéron et al., *Chem. Mater.*, **21**, 5607 (2009).
19. M. M. Thackeray et al., *Electrochemistry Communications*, **5**, 752 (2003).
20. N. V. Landschoot, E. M. Kelder, P. J. Kooyman, C. Kwakernaak, and J. Schoonman, *Journal of Power Sources*, **138**, 262 (2004).
21. J. S. Kim et al., *J. Electrochem. Soc.*, **151**, A1755 (2004).
22. Y. K. Sun, Y. S. Lee, M. Yoshio, and K. Amine, *Electrochem. Solid-State Lett.*, **5**, A99 (2002).
23. S.-T. Myung et al., *Chem. Mater.*, **17**, 3695 (2005).
24. J. Liu et al., *J. Electrochem. Soc.*, **154**, A55 (2007).
25. K. Edström, T. Gustafsson, and J. O. Thomas, *Electrochimica Acta*, **50**, 397 (2004).
26. E. Markevich, G. Salitra, and D. Aurbach, *Electrochemistry Communications*, **7**, 1298 (2005).

27. Y.-C. Lu, A. N. Mansour, N. Yabuuchi, and Y. Shao-Horn, *Chem. Mater.*, **21**, 4408 (2009).
28. A. T. Appapillai, A. N. Mansour, J. Cho, and Y. Shao-Horn, *Chem. Mater.*, **19**, 5748 (2007).
29. D. Aurbach, B. Markovsky, A. Shechter, Y. Ein Eli, and H. Cohen, *J. Electrochem. Soc.*, **143**, 3809 (1996).
30. S. Leroy, H. Martinez, R. Dedryvère, D. Lemordant, and D. Gonbeau, *Applied Surface Science*, **253**, 4895 (2007).
31. D. Briggs and J. T. Grant, *Surface Analysis by Auger and X-ray Photoelectron Spectroscopy*, IMP Publications and SurfaceSpectra, UK (2003).
32. S. Tanuma, C. J. Powell, and D. R. Penn, *Surface and interface analysis*, **20**, 77 (1993).
33. S. Tanuma, C. J. Powell, and D. R. Penn, *Surface and interface analysis*, **43**, 689 (2011).
34. Y. Ozawa, R. Yazami, and B. Fultz, *Electrochem. Solid-State Lett.*, **8**, A38 (2005).
35. D. Aurbach et al., *Journal of Power Sources*, **165**, 491 (2007).
36. R. Dedryvère et al., *Chem. Mater.*, **16**, 1056 (2004).
37. R. Dedryvère et al., *J. Phys. Chem. B*, **109**, 15868 (2005).
38. D. T. Clark and H. R. Thomas, *Journal of Polymer Science: Polymer Chemistry Edition*, **16**, 791 (1978).
39. C. D. Wagner et al., *Surface and interface analysis*, **3**, 211 (1981).
40. C. Battistoni, G. Mattogno, and E. Paparazzo, *Surface and interface analysis*, **7**, 117 (1985).
41. B. Philippe et al., *Chem. Mater.*, **24**, 1107 (2012).
42. B. Philippe et al., *J. Am. Chem. Soc.*, **135**, 9829 (2013).
43. C. V. Ramana, M. Massot, and C. M. Julien, *Surface and interface analysis*, **37**, 412 (2005).
44. C. V. Ramana et al., *J. Phys. Chem. C*, **111**, 1049 (2007).
45. W. E. Morgan, J. R. Van Wazer, and W. J. Stec, *J. Am. Chem. Soc.*, **95**, 751 (1973).
46. R. Alcántara et al., *Journal of Electroanalytical Chemistry*, **584**, 147 (2005).
47. G. M. Veith, N. J. Dudney, J. Howe, and J. Nanda, *J. Phys. Chem. C*, **115**, 14325 (2011).
48. L. El Ouatani, R. Dedryvère, C. Siret, and P. Biensan, *J. Electrochem. Soc.*, **156**, A468 (2009).
49. L. El Ouatani, R. Dedryvère, C. Siret, and P. Biensan, *J. Electrochem. Soc.*, **156**, A103 (2009).
50. J. C. Burns, N. N. Sinha, D. J. Coyle, and G. Jain, *J. Electrochem. Soc.*, **159**, A85 (2012).
51. J. W. Braithwaite, *J. Electrochem. Soc.*, **146**, 448 (1999).
52. H. Yang, K. Kwon, T. M. Devine, and J. W. Evans, *J. Electrochem. Soc.*, **147**, 4399 (2000).
53. K. Xu, *Chem. Rev.*, **104**, 4303 (2004).
54. B. J. Bachman and M. J. Vasile, *Journal of Vacuum Science & Technology A: Vacuum, Surfaces, and Films*, **7**, 2709 (1989).
55. B.-Y. Yu et al., *Anal. Chem.*, **80**, 3412 (2008).